Electric-field-induced second-harmonic generation mediated by one-dimensional excitons in polysilanes

H. Kishida
Department of Physics, The University of Tokyo, Tokyo 113, Japan
and Department of Applied Physics, The University of Tokyo, Tokyo 113, Japan

T. Hasegawa, Y. Iwasa, and T. Koda
Department of Applied Physics, The University of Tokyo, Tokyo 113, Japan

Y. Tokura
Department of Applied Physics, The University of Tokyo, Tokyo 113, Japan
and Joint Research Center for Atom Technology (JRCAT), Tsukuba, Ibaraki 305, Japan

H. Tachibana
Joint Research Center for Atom Technology (JRCAT), Tsukuba, Ibaraki 305, Japan
and National Institute of Materials and Chemical Research, Tsukuba, Ibaraki 305, Japan

M. Matsumoto
National Institute of Materials and Chemical Research, Tsukuba, Ibaraki 305, Japan

S. Wada, T. T. Lay, and H. Tashiro
The Institute of Physical and Chemical Research (RIKEN), Wako, Saitama 351-01, Japan
(Received 15 April 1994)

The third-order nonlinear-susceptibility $\chi^{(3)}(-2\omega;\omega,\omega,0)$ spectrum has been investigated for thin films of linear-Si-chain compounds, poly(dihexylsilane), by measurements of electric-field-induced second-harmonic generation (EFISHG). In the $\chi^{(3)}$ spectrum for EFISHG, two-photon resonance structures to the first and second levels of one-dimensional excitons were observed. The observed $\chi^{(3)}$ spectrum can be accounted for by considering multiple optical processes in the one-dimensional excitonic series characteristic of the Si-chain system.

I. INTRODUCTION

A picture of one-dimensional (1D) Wannier excitons has been successfully applied to elucidate optical properties of regular chains of polysilanes, which may be viewed as quantum wires made of Si.[1–3] In particular, it has been found that a nonlinear optical spectrum reflects the whole structure of the 1D exciton series and is characterized by each experimental configuration such as third-harmonic generation (THG) and electro-absorption that is relevant to the third-order nonlinear susceptibilities $\chi^{(3)}(-3\omega;\omega,\omega,\omega)$ (Refs. 2 and 4) and $\chi^{(3)}(-\omega;\omega,0,0)$ (Refs. 3 and 5), respectively. To pursue the full relationship between excitonic structures and nonlinear optical response in polysilanes, we have measured in the present study another important third-order nonlinear susceptibility, that is, $\chi^{(3)}(-2\omega;\omega,\omega,0)$, by the method of electric-field-induced second-harmonic generation (EFISHG).

The method of EFISHG has been generally used for measurements of nonlinear susceptibility, in which the roles of the applied electric field are different depending on the form of the sample. In liquid solutions, this method is employed to measure the second-order hyperpolarizability of the molecule with a permanent dipole. In this case, the applied electric field plays the role of aligning the permanent dipoles of the individual molecules and makes second-harmonic generation (SHG) detectable. In the gas phase, on the other hand, an applied electric field breaks the symmetry of electronic states in atoms[6] and molecules[7] and makes them second-harmonic active. In this case, the electrodes for the applied electric field can be arranged so that the sign of the applied electric field alternates periodically[8]. Thus, quasi-phase-matching can be achieved by alternating the polarity of the applied electric field every coherence length as well as by varying the gas pressure.

In solids, the electric field breaks the symmetry of the electronic state and hence makes it possible to generate second harmonics.[9] In the case of thin films of polymeric semiconductors, however, it was reported[10] that the photocarriers generated by photoexcitation move within the sample in a long time scale from seconds to minutes so as to reduce the effective electric field. Therefore the application of a static electric field is not suitable for nonlinear optical measurements of polymeric semiconductors. In order to avoid this problem, we used a low-frequency ($\sim$ 1 kHz) modulated electric field in the EFISHG experi-

ments to deduce $\chi^{(3)}(-2\omega;\omega,\omega,0)$ spectrum of polysilane films.

The polysilane investigated here is poly(dihexylsilane) (PDHS), which has two hexyl groups per one silicon atom as side groups as depicted in the inset of Fig. 3 below. Among various polysilanes, PDHS may be the most suitable system, since it shows a well-ordered regular chain with the *trans*-planar conformation of the Si backbone and shows a complete set of excitons below 5 eV (i.e., in the near uv region). Up to now, linear and nonlinear spectral data of PDHS (including one-photon and two-photon absorption,[1,4,11,12] electroabsorption,[3,5] and THG spectra[2,4]) have been accumulated for PDHS, which enables us to compare the present $\chi^{(3)}$ spectrum obtained by the EFISHG method with the other existing $\chi^{(3)}$ data and analyze them with a unified model.

II. EXPERIMENTAL PROCEDURE AND RESULTS

PDHS polymers were synthesized by the method of Wurtz coupling as described in detail elsewhere.[13] The films of polysilane were prepared by spin casting from heptane solution onto fused quartz substrates. (The fused quartz substrate generates no second harmonics). The thickness of the films was measured by a stylus profilometer. The homogenous thickness (120–400 nm) of each film can be controlled by the polymer concentration of the solution. We arranged two aluminum electrodes on this film by vapor deposition for the purpose of EFISHG measurements and the gap between the electrodes was about 1 mm.

Two types of exciting light source were used. One was a Xe-Cl excimer pumped dye laser operated at 570–800 nm with a pulse width of 15 ns. For the wavelength region beyond 750 nm, its output power dropped and was found insufficient for gaining enough second-harmonic signal intensities. Then we introduced the second laser system, in which emissions from a dye laser (572–628 nm) pumped with a frequency-doubled Nd:YAG laser (YAG is yttrium aluminum garnet) (pulse width 8 ns) were converted downward efficiently by a Raman shifter of H_2 (80 cm in cell length and about 5 atm in pressure). This system provided output pulse energies of more than several mJ in the 750–850 nm range. The exciting light beam from these laser systems was focused onto the sample region between the two electrodes. The polarization of the excitation beam was set parallel to the applied electric field. The second-harmonic signal generated was separated from the excitation beam by using bandpass filters and a monochromator. The signal was detected by a photomultiplier and processed by a boxcar integrator. To avoid a possible screening effect arising from photocarriers, we applied an alternating electric field at a frequency of 1.28 kHz. The repetition frequency of both laser systems were fixed at 10 Hz and the laser pulse was adjusted so as to coincide with the peaks of the applied ac electric field.

The nonlinear susceptibility of the sample was estimated by the Maker fringe method. A substrate of rock crystal (SiO_2) was used as a standard sample and the $\chi^{(3)}$ value of the sample was measured by comparing the second-harmonic intensity of rock crystal with the EFISH intensity of the sample. Substantially, the $\chi^{(3)}$ value was deduced using the relation

$$\chi^{(3)} = \frac{2}{3\pi}\frac{\alpha l/2}{\{1-\exp(-\alpha l/2)\}}\frac{l_c}{l}\sqrt{\frac{I_{\rm sam}}{I_{\rm sub}}}\frac{\chi_{\rm Q}^{(2)}}{E}. \quad (1)$$

Here l_c is the coherence length of the rock crystal, l the thickness of the thin film, $I_{\rm sam}$ the intensity of EFISH from the sample, $I_{\rm sub}$ the second-harmonic intensity from the rock crystal (reference), $\chi_{\rm Q}^{(2)}$ the second-order nonlinear susceptibility of the rock crystal, E the magnitude of the applied electric field, and α the absorption coefficient of the sample at the wavelength of the second harmonics. The $\chi^{(2)}$ spectrum of the rock crystal is calculated using Miller's rule[14] and the $\chi^{(2)}$ value at 1.064 μm which was reported by Roberts.[15]

The dependence of the second-harmonic intensity on the magnitude of the applied electric field and on the intensity of the incident light is shown in Figs. 1(a) and 1(b), respectively. The second-harmonic intensity was observed to be proportional to the square of the magnitude of the applied electric field and the square of the intensity of incident light. This ensures that the detected signal was certainly caused by the nonlinearity $\chi^{(3)}(-2\omega;\omega,\omega,0)$ of the sample since these observations were consistent with the following relations:

$$\begin{aligned} I(2\omega) &\propto [E(2\omega)]^2 \\ &\propto [\chi^{(3)}(-2\omega;\omega,\omega,0)E(\omega)E(\omega)E(0)]^2 \\ &\propto [\chi^{(3)}(-2\omega;\omega,\omega,0)]^2 I(\omega)^2 E(0)^2. \end{aligned} \quad (2)$$

Here, $I(2\omega)$ and $I(\omega)$ are the intensity of second-harmonic and fundamental laser light, respectively; $E(2\omega)$ and $E(\omega)$ are the amplitude of the electric field of second-harmonic and fundamental laser beam, respec-

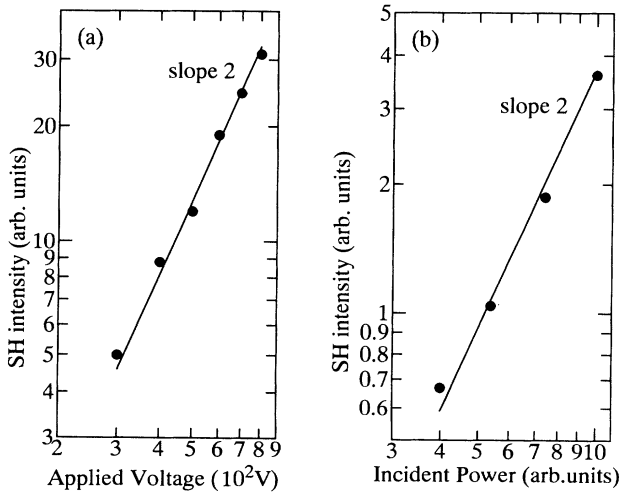

FIG. 1. (a) Dependence of the EFISH intensity on the amplitude of the applied electric field (1.28 kHz). (b) Dependence of the EFISH intensity on the incident laser power. Fundamental photon energy is 2.17 eV in both runs.

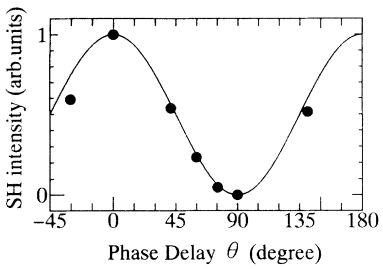

FIG. 2. Dependence of the EFISH intensity on the phase delay of the laser pulse to the applied ac (1.28 kHz) electric field. Experimental results (filled circles) are compared with the curve of the squared intensity of the applied electric field (solid line). The fundamental photon energy is 1.77 eV.

tively, and $E(0)$ is the quasi-dc electric field.

In Fig. 2 we show the dependence of EFISH intensity on the phase delay of the laser pulse to the applied electric field. The intensity of the EFISH was measured varying the phase delay θ of the laser pulse. (We set θ=0 when the intensity of the applied electric field reaches the maximum.) The solid line in the figure shows the square of the applied electric field intensity and the filled circles the measured values of the EFISH intensity. As clearly seen in Fig. 2, the EFISH intensity is proportional to the square of the applied electric field without phase difference, indicating that there is no phase difference between the applied electric field and the effective electric field. Thus the presently observed results are totally free from the slow dynamics of photocarriers.

The $|\chi^{(3)}(-2\omega;\omega,\omega,0)|$ spectrum of PDHS film, which was measured by the above-described EFISHG method, is shown in Fig. 3(b). A sharp resonant peak is observed

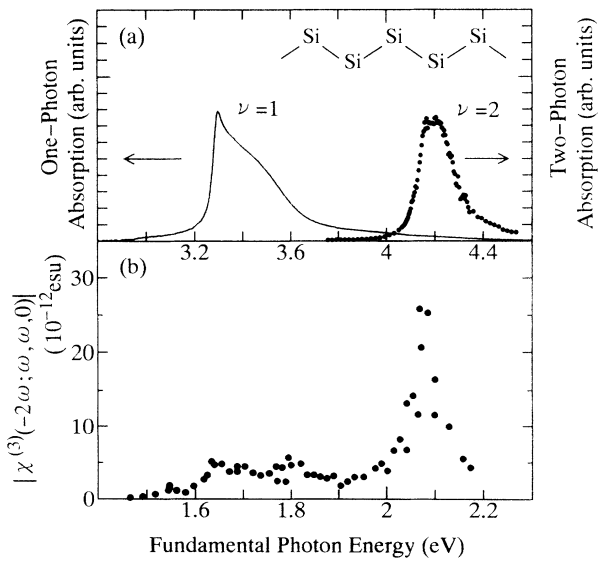

FIG. 3. Spectra of (a) one-photon absorption (solid line) and two-photon absorption (dots), and (b) EFISH $|\chi^{(3)}(-2\omega;\omega,\omega,0)|$ of poly(dihexylsilane) (PDHS) film at room temperature.

around 2.09 eV, while a hump structure also shows up around 1.65 eV. For comparison, we show in Fig. 3(a) the one-photon and two-photon absorption spectra. The two-photon absorption spectra were measured by monitoring the intensity of the two-photon excited luminescence, as described elsewhere.[1] The origins of both resonant structures in the $|\chi^{(3)}(-2\omega;\omega,\omega,0)|$ spectrum can be interpreted in terms of the two-photon resonance, since there is no excited state in the fundamental photon energy region (1.4–2.2 eV) with which one-photon resonance can occur. By comparison of the spectra shown in Figs. 3(a) and 3(b), the sharp peak at 2.09 eV is assigned to a two-photon resonance to the two-photon allowed (^1A_g) state (4.19 eV) which shows up in the two-photon absorption spectrum. On the other hand, the hump structure at 1.65 eV may correspond to a two-photon resonance to the one-photon allowed ($^1B_{1u}$) state (3.30 eV) appearing in the one-photon absorption spectrum. Since the applied electric field perturbs the parity of the excited state and relaxes the selection rule, two-photon resonance is possible with both the $^1B_{1u}$ (one-photon allowed) and ^1A_g (two-photon allowed) states.

III. ANALYSIS BY THE ONE-DIMENSIONAL (1D) EXCITON MODEL

Before going to the discussion of the $\chi^{(3)}$ spectrum, let us first elucidate the excitonic features characteristic of the PDHS chains. One- and two-photon absorption spectra [Fig. 3(a)] have been well accounted for in terms of the one-dimensional (1D) exciton model.[1,3,16–18] The backbone of polysilane can be viewed as a 1D semiconductor composed of 1D valence and conduction bands. In such a 1D system, the excited electron and hole are tightly bound by the Coulomb interaction to form 1D excitons. The relative motion of a hole and an electron in 1D exciton states bears a close analogy to the problem of the 1D hydrogen atom.[19] In fact, the 1D excitonic states of PDHS have been extensively investigated experimentally[1–3] and theoretically[18] in terms of the 1D semiconductor model. We show schematics for the excitonic levels and the envelope functions in Fig. 4. Since the single polymer chain has D_{2h} symmetry, every singlet state is classified as either $^1B_{1u}$ or ^1A_g. As seen in Fig. 4, the lowest exciton state ($\nu = 1$) is $^1B_{1u}$, to which a one-photon transition is allowed from the ground state (^1A_g). The second exciton state ($\nu = 2$) has the symmetry of ^1A_g, which is one-photon forbidden but two-photon allowed. As reported in previous studies[2,3] and also demonstrated in the following part of this paper, there are experimental implications that the third exciton state ($\nu = 3$) with $^1B_{1u}$ symmetry lies close above the $\nu = 2$ exciton. Thus the 1D excitonic states consist of an alternating series of even and odd parity states.

To understand the shape of the $|\chi^{(3)}(-2\omega;\omega,\omega,0)|$ spectrum, multiphoton processes mediated by such 1D excitonic states and their superposition are important. Hereafter we compare the experimental spectra with the spectra calculated by the tight-binding model and estimate the respective contribution of exciton-mediated multiphoton processes to the total $\chi^{(3)}$ spectral shape.

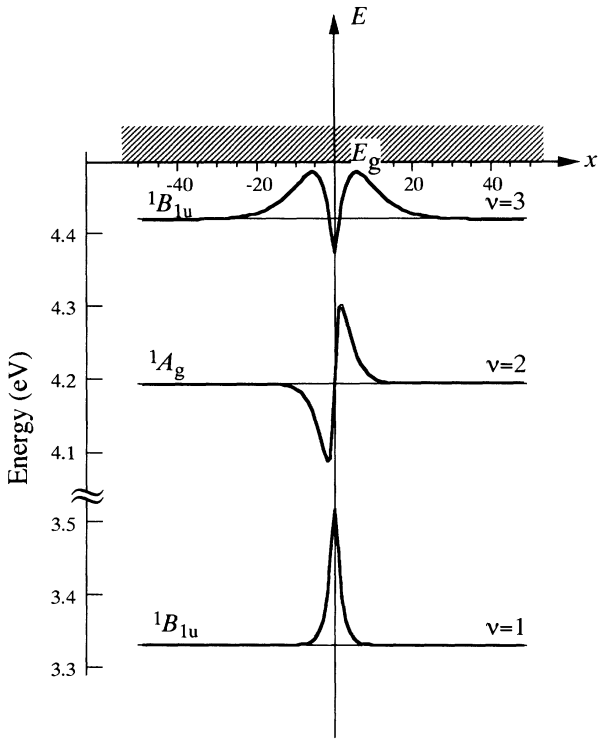

FIG. 4. Envelope functions of the 1D excitons. The abscissa (x) is the distance between the hole and electron of the exciton in units of the lattice constant and the horizontal level of each ordinate for the envelope function indicates the energy of the exciton. The hatched part above E_g (band gap) represents the electron-hole continuum.

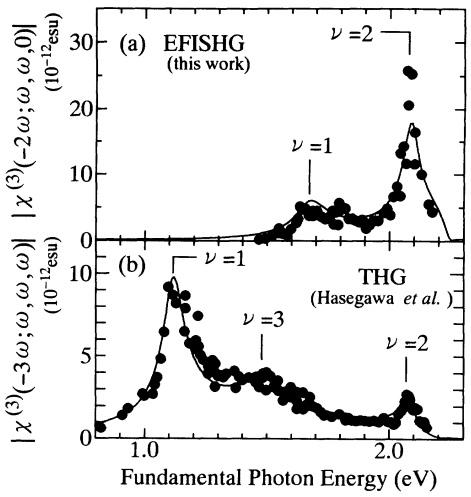

FIG. 5. Experimental spectra (circles) of (a) $|\chi^{(3)}(-2\omega;\omega,\omega,0)|$ and (b) $|\chi^{(3)}(-3\omega;\omega,\omega,\omega)|$ in comparison with the corresponding spectra (solid lines) calculated by the tight-binding model with a single CI procedure using the same set of parameters (see text).

In Fig. 5(a), we compare the observed $\chi^{(3)}$ spectrum with the one calculated by the tight-binding model with a long-range Coulomb potential. The main body of the present calculation is that developed by Abe *et al.*,[16–18] the essence of which is as follows. Two sp^3 orbitals pointing toward the neighboring Si site were chosen out of the four sp^3 orbitals of one Si atom as bases of the 1D electronic state on the σ-bonded chain. One-electron states (or one-electron bands) are calculated from these bases. Then, one-electron excited states between these levels (bands) are diagonalized with respect to the electron-electron interaction. In the calculation, the electronic parameters are t_v, the transfer energy between sp^3 orbitals belonging to another vicinal Si atom, t_g, the transfer energy between two sp^3 orbitals belonging to the same Si atom, U, the on-site Coulomb potential, V the intersite Coulomb potential, and $V_{ij}(=V/|i-j|$ for $i \neq j)$ the long-range Coulomb potential between the ith and jth sites. The excited states calculated by a single configuration-interaction (CI) procedure are regarded as the 1D excitonic states. The detailed procedure of the calculation was described in the paper by Abe *et al.*[18] Using these excitonic states, nonlinear susceptibility was calculated by the diagrammatic perturbation theory.[20] The values of the parameters used here were t_v=2.1 eV, t_g=0.84 eV, U=4.9 eV, V=2.45 eV, and the site number is N=400 as an approximation of an infinite chain. The envelope functions calculated for the lower-lying excitons (ν=1–3) are the ones depicted already in Fig. 4.

A comparison between the calculated and observed spectra is shown in Fig. 5(a). The agreement between the calculated (solid line) and observed spectra is fairly good.[21] In the observed spectra, the two-photon resonant peak to the $\nu = 2$ exciton at 2.09 eV is much more prominent than the resonant peak to the $\nu = 1$ exciton around 1.65 eV. This characteristic feature in EFISHG is well reproduced by the calculated spectra. Using the same set of electronic parameters, we have also calculated the $|\chi^{(3)}(-3\omega;\omega,\omega,\omega)|$ spectrum for the THG configuration, and compared it with the experimental $|\chi^{(3)}(-3\omega;\omega,\omega,\omega)|$ spectrum reported by Hasegawa *et al.*[2] [Fig. 5(b)]. The same set of parameters can satisfactorily reproduce the experimental $\chi^{(3)}$ spectra for both THG and EFISHG configurations.

IV. MULTIPHOTON RESONANT PROCESS MEDIATED BY 1D EXCITONS

The multiphoton resonant structures showing up in the THG $\chi^{(3)}$ spectrum are quite different from those of the EFISHG $\chi^{(3)}$ spectrum. The three structures seen in the THG $\chi^{(3)}$ spectrum have been assigned (in order of increasing energy) to a three-photon resonant peak with the $\nu = 1$ exciton, a three-photon resonant structure with the $\nu \geq 3$ excitons, and a two-photon resonant structure to the $\nu = 2$ state, respectively.[2] In the THG $\chi^{(3)}$ spectrum, the three-photon resonant peak with the $\nu = 1$ exciton is much larger than the two-photon resonant peak with the $\nu = 2$ exciton, which is in contrast to the case of the EFISHG $\chi^{(3)}$ spectrum. The difference in the relative magnitudes of these resonant peaks bears an important implication with regard to the respective nonlinear optical processes in THG and EFISHG. To clarify this point, let us hereafter decompose the nonlinear optical process into the respective dominant terms, taking account of the ground state ($\nu = 0$) and three exciton states (ν =1,

2, and 3) (Fig. 6). These states are in fact the "*essential states*" in the process, as shown in the following, in accord with the arguments developed by Dixit *et al.*[22]

Since the third-order nonlinear optical process is a four-photon process, we have to treat various combinations of four levels of the 1D excitonic states (including the ground state). Among the four-photon optical processes within the four levels shown in Fig. 6, the most dominant one is the transition $\nu = 0 \rightarrow 1 \rightarrow 2 \rightarrow 1 \rightarrow 0$ (denoted hereafter as $\langle 01210 \rangle$). In addition, there are other transitions to be taken into account. They are expressed as $\langle 01230 \rangle$ (or equivalently $\langle 03210 \rangle$) and $\langle 03230 \rangle$ using the same abbreviation as $\langle 01210 \rangle$. However, the process $\langle 03230 \rangle$, which does not involve the $\nu = 1$ exciton, contributes much less to $\chi^{(3)}$, since the transition dipole moment between the ground state and the $\nu = 3$ state ($^1B_{1u}$) is very small as compared with that for the $\nu = 1$ $^1B_{1u}$ exciton[2] and such a process must include the product of the small dipole moments. Therefore we will focus here on the real and imaginary component of $\chi^{(3)}$ contributed from the two transitions $\langle 01210 \rangle$ and $\langle 01230 \rangle$, denoted, respectively, as $\chi^{(3)}_{01210}$ and $\chi^{(3)}_{01230}$, in particular, on the phase relation between $\chi^{(3)}_{01210}$ and $\chi^{(3)}_{01230}$.

Around the two-photon resonant peak with the $\nu = 2$ exciton, the contributions of $\chi^{(3)}_{01210}$ and $\chi^{(3)}_{01230}$ in the THG process have opposite signs both in the real and imaginary parts, whereas the signs are the same in the EFISHG process. As a result, their contributions tend to be cancelled in THG, while they are reinforced in EFISHG around the $\nu = 2$ peak. The reason why the signs are opposite for the respective $\chi^{(3)}$ processes can be accounted for by taking into consideration the most dominant terms in $\chi^{(3)}_{01210}$ and $\chi^{(3)}_{01230}$ for THG and EFISHG, denoted, respectively, as $\chi^{(3)}_{01210d}$ and $\chi^{(3)}_{01230d}$. We show in Fig. 7 the spectra of the $\chi^{(3)}_{01210d}$ and $\chi^{(3)}_{01230d}$, which were calculated by the expressions,

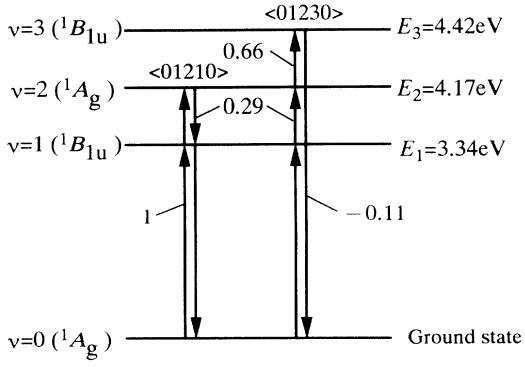

FIG. 6. Four-level model in the 1D exciton system. $\langle 01210 \rangle$ and $\langle 01230 \rangle$ are the dominant four-photon processes in the 1D excitonic system. E_ν ($\equiv \hbar\omega_{0\nu}$) is the energy of the νth exciton state. The transition dipole moments are indicated in units of $\langle 0|x|1 \rangle$.

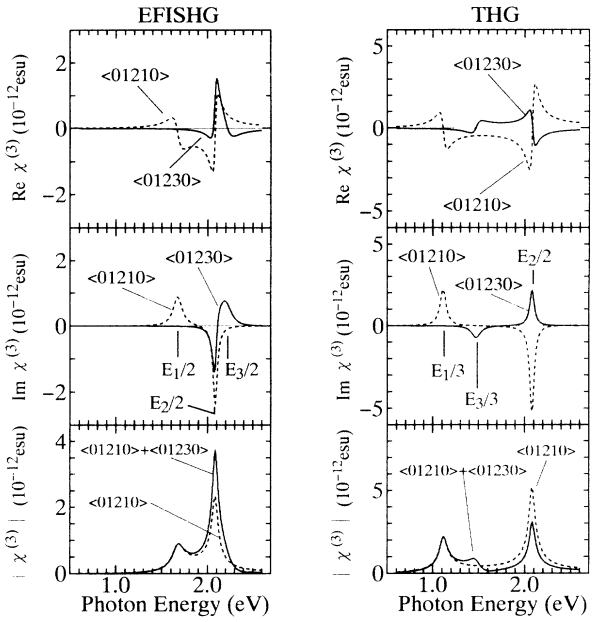

FIG. 7. Real and imaginary parts as well as the absolute values of the dominant components of $\chi^{(3)}$ in THG and EFISHG in terms of the four-level model. Contributions from the dominant processes are shown by solid and broken curves (see text). E_ν ($\equiv \hbar\omega_{0\nu}$) is the energy of the νth exciton state. The positions of the fundamental photon energy of two- and three-photon resonance with the νth exciton state are indicated as $E_\nu/2$ and $E_\nu/3$, respectively.

$$\chi^{(3)}_{01210d}(\omega) \propto \frac{\langle 0|x|1\rangle\langle 1|x|2\rangle\langle 2|x|1\rangle\langle 1|x|0\rangle}{(\omega_{01} - \omega - i\Gamma_1)(\omega_{02} - 2\omega - i\Gamma_2)(\omega_{01} - \omega_h - i\Gamma_1)}, \tag{3}$$

$$\chi^{(3)}_{01230d}(\omega) \propto \frac{\langle 0|x|1\rangle\langle 1|x|2\rangle\langle 2|x|3\rangle\langle 3|x|0\rangle}{(\omega_{01} - \omega - i\Gamma_1)(\omega_{02} - 2\omega - i\Gamma_2)(\omega_{03} - \omega_h - i\Gamma_3)}. \tag{4}$$

Here, ω is the frequency of the incident light, ω_{mn} the frequency difference between the mth and nth states, ω_h the frequency of the generated harmonic (i.e., $\omega_h = 2\omega$ in EFISHG and $\omega_h = 3\omega$ in THG), $\langle m|x|n \rangle$ the transition dipole moment between the mth and nth states, and Γ_i the damping constant of the ith state. For calculation, the respective matrix elements and damping constant Γ_i were assumed to be the same as used in the aforementioned tight-binding model.

For evaluation of the complex components of $\chi^{(3)}_{01210d}$ and $\chi^{(3)}_{01230d}$, it is important to consider the sign of the matrix elements and the phase of the energy denominator on the complex plane. The sign of the matrix ele-

ment can easily be deduced from the shape of the envelope function of the 1D excitons (Fig. 4). The sign of the transition dipole moment between the ground state $|0\rangle$ and νth excitonic state is identical with the sign of the envelope function of the νth state at the origin $x = 0$, while that between excitonic states can be determined by the integral of the product of the two excitonic envelope functions and the potential x. For example, the product $\langle 0|x|1\rangle\langle 1|x|2\rangle\langle 2|x|1\rangle\langle 1|x|0\rangle$ is positive and $\langle 0|x|1\rangle\langle 1|x|2\rangle\langle 2|x|3\rangle\langle 3|x|0\rangle$ is negative. As for the phase of the energy denominator, there is a change of $-\pi$ across each resonance.

In the dominant term of $\langle 01210\rangle$ (see broken curves in Fig. 7), the lowest resonance peak is attributable to the resonance with the $\nu = 1$ state both in THG and in EFISHG (a three-photon resonance in THG and a two-photon resonance in EFISHG). This peak is followed by the second resonance with the $\nu = 2$ state (a two-photon resonance) in both THG and EFISHG). In the dominant term of $\langle 01230\rangle$ (solid curves in Fig. 7), on the other hand, the peaks in THG successively occur due to the three-photon resonance with the $\nu = 3$ state and two-photon resonance with the $\nu = 2$ state, while those in EFISHG are due to the two-photon resonances with the $\nu = 2$ and $\nu = 3$ states in order of increasing energy.

To sum up, the two-photon resonance with the $\nu = 2$ state for the THG configuration is the second resonance for both $\langle 01210\rangle$ and $\langle 01230\rangle$, but the signs of these matrix elements are opposite. Therefore the resonance peak with the $\nu = 2$ state in THG is suppressed by contribution from the $\nu = 3$ exciton state. In EFISHG, the two-photon resonance with the $\nu = 2$ state is the second resonance in $\langle 01210\rangle$ and the first one in $\langle 01230\rangle$, yet the signs of these matrix elements are opposite. Thus, the resonance peak with the $\nu = 2$ state is enhanced by the $\nu = 3$ exciton state in EFISHG, which is contrary to the case of THG.

In Fig. 7, we have also plotted the $|\chi^{(3)}|$ spectra which were calculated with the dominant term of the $\langle 01210\rangle$ process alone and with the dominant terms of both the $\langle 01210\rangle$ and $\langle 01230\rangle$ processes. The latter four-level model can account for the essential features in the $\chi^{(3)}$ spectra, whereas the former three-level model obviously fails to account for the resonant spectral shapes and their differences in the observed $\chi^{(3)}(-2\omega;\omega,\omega,0)$ and $\chi^{(3)}(-3\omega;\omega,\omega,\omega)$ spectra.

In terms of the interfering multiphoton processes involving the $\nu = 3$ exciton state, we can thus give a reasonable explanation for the experimental result that the two-photon resonance peak with the $\nu = 2$ state is significantly enhanced in EFISHG, whereas it is suppressed in THG. The higher levels above the $\nu = 3$ exciton were omitted from consideration in the above four-level model, but they must give essentially the same effect as the $\nu = 3$ exciton and further enhance the difference in the resonant structure of $|\chi^{(3)}(-2\omega;\omega,\omega,0)|$ and $|\chi^{(3)}(-3\omega;\omega,\omega,\omega)|$. In fact, all the 1D excitonic levels have been included in the calculations of $|\chi^{(3)}(-3\omega;\omega,\omega,\omega)|$ and $|\chi^{(3)}(-2\omega;\omega,\omega,0)|$ shown in Fig. 5. Thus, the higher-lying exciton states, which can hardly be detected in the conventional one- and two-photon absorption spectra, make an important contribution to the resonant structures in the nonlinear-susceptibility spectra.

V. SUMMARY

We have measured the third-order nonlinear susceptibility $|\chi^{(3)}(-2\omega;\omega,\omega,0)|$ of *trans*-planar polysilane, PDHS, by the method of electric-field-induced second-harmonic generation (EFISHG). In the observed $|\chi^{(3)}|$ spectrum, two resonant structures were found to be prominent, one being an intense peak arising from the two-photon resonance with the one-photon forbidden state (the $\nu = 2$ exciton state), the other being a hump structure due to the two-photon resonance with the one-photon allowed lowest excited state (the $\nu = 1$ exciton state). Comparing the experimental results with the theoretical spectra calculated by the tight-binding model with a long-range Coulomb interaction, we have found that the nonlinear-susceptibility spectra are sensitively affected by the superposition of interfering multiphoton processes in the 1D excitonic system. Resonant structures in the experimental THG and EFISHG $\chi^{(3)}$ spectra as well as their different characteristics can be consistently accounted for by the enhancement or suppression relevant to the higher ($\nu \geq 3$) exciton states.

ACKNOWLEDGMENTS

We are grateful to S. Abe for enlightening discussion. We also thank A. Makimoto and S. Yasukawa for collaboration in the calculation and experiments of the nonlinear optical spectra. This work was supported in part by a Grant-In-Aid for Scientific Research from the Ministry of Education, Science and Culture in Japan, the Nissan Science Foundation, and the NEDO Foundation, Japan.

[1] Y. Moritomo, Y. Tokura, H. Tachibana, Y. Kawabata, and R. D. Miller, Phys. Rev. B **43**, 14746 (1991).
[2] T. Hasegawa, Y. Iwasa, H. Sunamura, T. Koda, Y. Tokura, H. Tachibana, M. Matsumoto, and S. Abe, Phys. Rev. Lett. **69**, 668 (1992).
[3] H. Tachibana, M. Matsumoto, Y. Tokura, Y. Moritomo, A. Yamaguchi, S. Koshihara, R. D. Miller, and S. Abe, Phys. Rev. B **47**, 4363 (1993).
[4] T. Hasegawa, Y. Iwasa, H. Kishida, T. Koda, Y. Tokura, H. Tachibana, and Y. Kawabata, Phys. Rev. B **45**, 6317 (1992).
[5] H. Tachibana, Y. Kawabata, S. Koshihara, and Y. Tokura, Solid State Commun. **75**, 5 (1990).
[6] R. S. Finn and J. F. Ward, Phys. Rev. Lett. **6**, 285 (1971).
[7] J. F. Ward and D. S. Elliott, J. Chem. Phys. **69**, 5438 (1978).

[8] D. P. Shelton and A. D. Buckingham, Phys. Rev. A **26**, 2787 (1982).
[9] R. W. Terhune, P. D. Maker, and C. M. Savage, Phys. Rev. Lett. **8**, 404 (1962).
[10] P. A. Chollet, P. Kajzar, and J. Messier, Thin Solid Films **132**, 1 (1985).
[11] J. R. G. Thorne, Y. Ohsako, J. M. Zeigler, and R. M. Hochstrasser, Chem. Phys. Lett. **162**, 455 (1989).
[12] Z. G. Soos and R. G. Kepler, Phys. Rev. B **43**, 11 908 (1991).
[13] R. D. Miller and J. Michl, Chem. Rev. **89**, 1359 (1989).
[14] R. C. Miller, Appl. Phys. Lett. **5**, 17 (1964).
[15] D. A. Roberts, IEEE J. Quantum Electron. **28**, 2057 (1992).
[16] S. Abe, J. Phys. Soc. Jpn. **58**, 62 (1989).
[17] S. Abe, M. Schreiber, W. P. Su, and J. Yu, Phys. Rev. B **45**, 9432 (1992).
[18] S. Abe, M. Schreiber, and W. -P. Su, Chem. Phys. Lett. **192**, 425 (1992).
[19] R. Loudon, Am. J. Phys. **27**, 649 (1959).
[20] J. F. Ward, Rev. Mod. Phys. **37**, 1 (1965).
[21] The calculated spectrum in each experimental configuration, which is obtained for an isolated single chain, actually a spectrum of "molecular" hyperpolarizability, was multiplied by a constant to fit the experimental spectrum for the polymer films. This constant should reflect the electric field for the individual polymer chains in each experimental configuration, although the precise estimate of this constant is difficult. We dealt with this constant as a fitting parameter.
[22] S. N. Dixit, D. Guo, and S. Mazumdar, Phys. Rev. B **43**, 6781 (1991).